Effects of Milling in Hydrogen on Magnesium Hydride with a Hydride-Forming Titanium Additive

Myoung Youp SONG [1]*, Eunho CHOI [2]

[1] *Division of Advanced Materials Engineering, Hydrogen & Fuel Cell Research Center, Engineering Research Institute, Jeonbuk National University, 567 Baekje-daero Deokjin-gu Jeonju, 54896, Republic of Korea*
[2] *Department of Materials Engineering, Graduate School, Jeonbuk National University, 567 Baekje-daero Deokjin-gu Jeonju, 54896, Republic of Korea*

A hydride-forming element titanium (Ti) was selected as an additive to improve the hydrogen uptake and release properties of MgH_2. The hydrogen uptake and release properties of three Ti-added MgH_2 alloys [named MgH_2-xTi (x = 6, 12, and 15)] prepared by milling in hydrogen (reactive mechanical grinding) were investigated and those of MgH_2-12Ti were studied in more detail because it had the highest initial hydrogen uptake and release rates and the largest quantities of hydrogen absorbed and released for 60 min. At the cycle number, n, of one ($n = 1$), MgH_2-12Ti absorbed 4.01 wt.% H for 2.5 min and 6.39 wt.% H for 60 min at 573 K in 12 bar H_2, having an effective hydrogen storage capacity of 6.39 wt.%. MgH_2-12Ti released 0.44 wt.% H for 2.5 min and 1.86 wt.% H for 60 min at 593 K in 1.0 bar H_2. γ-MgH_2, $TiH_{1.924}$, and MgO were formed during reactive mechanical grinding. We believe that the brute forces and tensile, compressive, or shear stresses, which are applied to the materials during reactive mechanical grinding, introduce imperfections, fabricate cracks, expose fresh and clean surfaces, decrease the particle size, and disperse the additive among the particles. The γ-MgH_2, $TiH_{1.924}$, and MgO formed during reactive mechanical grinding and their pulverization during reactive mechanical grinding are believed to make these effects stronger.

Keywords: hydrogen absorbing materials, mechanical alloying/milling, scanning electron microscopy (SEM), X-ray diffraction, Ti-added MgH_2 alloy.

1. INTRODUCTION

Many studies have investigated magnesium hydride (MgH_2) as a promising hydrogen-storage medium for coming transportation, because magnesium hydride has a high hydrogen storage density and is relatively inexpensive. One of the obstacles to applying MgH_2 to a practical solid-state hydrogen-storage medium is its slow hydrogenation and dehydrogenation kinetics; high temperature is required for hydrogenation and dehydrogenation and reaction rates are low even at relatively high temperatures.

In order to improve the hydrogenation and dehydrogenation kinetics of magnesium (Mg), many researches have been performed adding catalysts [1 – 5], using various treatment methods of Mg, and synthesizing Mg-containing compounds [6]. Titanium (Ti) as a catalyst was added to MgH_2 [7, 8] or Mg [9 – 17]. Mechanical milling in argon was used by Liang et al. [1] to prepare MgH_2–Tm (Tm = 3d-transition elements Ti, V, Mn, Fe, Ni) nanocomposite powders. The composites with Ti or V additives showed very rapid desorption kinetics above 523 K and absorption kinetics at temperatures as low as 320 K. They reported that the activation energy of desorption for magnesium hydride was reduced drastically, whereas formation enthalpy and entropy of magnesium hydride were not altered by milling with transition metals. Mg–Ti–H FCC hydrides with a face centered cubic (FCC)

structure were synthesized directly by Asano et al. [8] from MgH_2 and Ti by means of ball milling. They reported that the Mg–Ti–H FCC hydride phases synthesized had chemical formulae of $Mg_{40}Ti_{60}H_{113}$ and $Mg_{29}Ti_{71}H_{57}$, corresponding to the hydrogen contents of 2.9 and 1.4 mass %, respectively. Titanium isopropoxide ($Ti[OCH(CH_3)_2]_4$) was also added to milled MgH_2 by Alsabawi et al. [18] to improve the reaction kinetics of Mg with hydrogen. They reported that the milling environment had little or no effect on the desorption kinetics in most cases but in some cases, the absorption uptake differed by up to 2 wt.%, depending on the gas used. They argued that all information about the ball-milling processes used, including the gas environment, must be reported. Korablov et al. [9] studied the kinetics and thermodynamics of hydrogenation-dehydrogenation for Mg-25%TM (TM = Ti, Nb or V) composites synthesized by reactive ball milling in hydrogen. They reported that for the dehydrogenation process, titanium was the best among the examined additives, as evidenced by its lowest activation energy of the hydrogen desorption $E_a = 53.6$ kJ/mol. To overcome sluggish kinetics, Rizo-Acosta et al. [10] added different Ti amounts ($y = 0$, 0.025, 0.05, 0.1, 0.2, and 0.3) to magnesium to form $(1-y)MgH_2+yTiH_2$ nanocomposites (NC) by reactive ball milling in hydrogen gas. As Ti amount increased, absorption and desorption kinetics were improved. However, the addition of titanium increased the molar weight of NCs and Ti formed irreversible titanium hydride. Maweja et al. [11] reported that the solid solubility of 50 at % Mg + 50 at % Ti powder mixtures was achieved by means of milling in a horizontal high

---
* Corresponding author. Tel.: +82-63-270-2379; fax: +82-63-270-2386.
E-mail address: *songmy@jbnu.ac.kr* (M.Y. Song)

energy ball. They reported that FCC and BCC matrices of Ti solid solution existed in Mg together with traces of an HCP Ti-rich phase after milling at 800 rpm for 48 and 72 h, respectively. The crystallite boundaries acted as preferential sites for the heterogeneous nucleation of the twins and for the formation of the solid solution by release of the lattice strain energy. Korablov et al. [12] synthesized Mg–Ti–H samples with an FCC structure mechano-chemically by ball milling in argon atmosphere or under elevated hydrogen pressure, using a metal as the reactant. A ternary Ti–Mg–H compound was not formed using metal hydrides (MgH_2 and TiH_2) as reactants. The amount of β-MgH_2 increased during the first hydrogen absorption cycle at 573 K at the expense of the high-pressure polymorph, γ-MgH_2, and the amount of β-MgH_2 remained constant during the following hydrogenations. Fast absorption–desorption kinetics at 573 K and lower onset temperatures for hydrogen release were observed for all investigated samples (lowest onset temperature of desorption of 490 K). In other works, Ti [13, 14], Ti and/or TiH_2 [15, 16], and TiH_2 and TiO_2 [17] were added to Mg to improve the reaction kinetics of Mg with hydrogen.

Many works to improve the hydrogenation and dehydrogenation kinetics of Mg were performed by adding titanium (Ti) to Mg [9 – 17], but a few works were done by adding Ti to MgH_2 [7, 8]. In the present work, a hydride-forming element Ti was chosen as an additive to MgH_2 to develop a Mg-based material with a hydrogen storage capacity over 6 wt.%. 6, 12, and 15 weight percent Ti were added to MgH_2 by milling in hydrogen (reactive mechanical grinding). The effects of milling in hydrogen on MgH_2 with a hydride-forming Ti additive were studied. And the hydrogen uptake and release properties of the Ti-added MgH_2 alloys [named MgH_2-xTi (x = 6, 12, and 15)] were investigated. In particular, the hydrogen uptake and release properties of MgH_2-12Ti were studied in more detail because it had the highest initial hydrogen uptake and release rates and the largest quantities of hydrogen absorbed and released for 60 min.

2. EXPERIMENTAL DETAILS

MgH_2 powder (Magnesium hydride, hydrogen storage grade, Sigma Aldrich.) and titanium (− 3.25 mesh, 99.5 % metal basis, Alfa Aesar) were used as starting materials.

Reactive mechanical grinding (RMG) to prepare MgH_2-xTi (x = 6, 12, and 15) was performed in a planetary ball mill (Planetary Mono Mill; Pulverisette 6, Fritsch). Samples with the desired compositions (total weight = 8 g) were mixed in a hermetically sealed stainless steel container with 105 hardened steel balls (total weight = 360 g); the sample to ball weight ratio was 1/45. All sample handling was performed in a glove box in Ar in order to prevent oxidation. The disc revolution speed was 250 rpm. The mill container (volume of 250 mL) was then filled with high purity hydrogen gas (~ 12 bar). Milling was performed for 6 h, during which the mill container was refilled with hydrogen every two hours.

The absorbed or released hydrogen quantity was measured as a function of time (*t*) in nearly constant hydrogen pressures (12 bar H_2 for hydrogen uptake and 1.0 bar H_2 for hydrogen release) using the volumetric

method, with the Sieverts' type hydrogen uptake and release apparatus described previously [19, 20]. For the hydrogen uptake measurement of the next cycle, vacuum pumping was done for 1.5 h at 623 K after every hydrogen release measurement. 0.5 g of the samples was used for these measurements.

Samples after reactive mechanical grinding and after hydrogen uptake-release cycling were characterized by X-ray diffraction (XRD) with Cu Kα radiation, using a Rigaku D/MAX 2500 powder diffractometer. The microstructures of the powders were observed using a JSM-5900 scanning electron microscope (SEM) operated at 20 kV.

3. RESULTS AND DISCUSSION

The quantities of hydrogen absorbed (H_a) and desorbed (released) (H_d) were calculated using the sample weight as a standard and expressed in the unit of wt.% H. The initial hydrogen uptake and release rates (wt.% H/min) were defined as the quantities of hydrogen absorbed and released, respectively, for the first 2.5 min divided by 2.5 min. The hydrogen uptake rate and the hydrogen release rate were defined as the tangents of the curves at given times. The quantities of hydrogen absorbed and released for *t* min were expressed as H_a (*t* min) and H_d (*t* min), respectively.

Fig. 1 shows the variation in the H_a vs. time *t* curve with x at 573 K in 12 bar H_2 at the cycle number, *n*, of one (*n* = 1) for MgH_2-xTi (x = 6, 12, and 15) samples. The initial hydrogen uptake rates of the samples are quite high and the hydrogen uptake rate becomes very low after about 15 min. MgH_2-12Ti has the highest initial hydrogen uptake rate and the largest quantity of hydrogen absorbed for 60 min, H_a (60 min), followed in order by MgH_2-6Ti and MgH_2-15Ti. MgH_2-12Ti absorbs 4.01 wt.% H for 2.5 min and 6.39 wt.% H for 60 min. Table 1 shows the variation of H_a with *t* at 573 K in 12 bar H_2 at *n* = 1 for MgH_2-xTi (x = 6, 12, and 15).
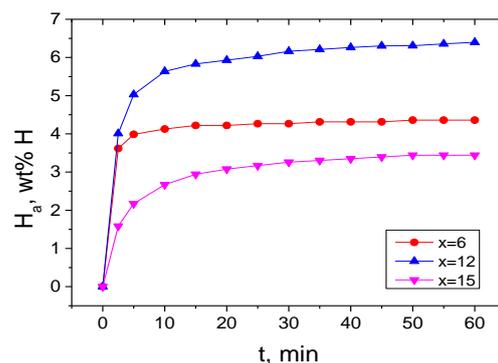
Fig. 1. Variation in the H_a vs. time *t* curve with x at 573 K in 12 bar H_2 at the first cycle (*n* = 1) for MgH_2-xTi (x = 6, 12, and 15) samples

Table 1. Variation of H_a (wt.% H) with *t* (min) at 573 K in 12 bar H_2 at *n* = 1 ~ 4 for MgH_2-xTi (x = 6, 12, and 15)

	2.5 min	5 min	10 min	30 min	60 min
x = 6	3.61	3.99	4.12	4.27	4.36
x = 12	4.01	5.03	5.63	6.16	6.39
x = 15	1.58	2.17	2.67	3.26	3.44

The variation in the H_d vs. t curve with x at 573 K in 1.0 bar H_2 at $n = 1$ for MgH$_2$-xTi (x = 6, 12, and 15) samples is shown in Fig. 2. The initial hydrogen release rates are slightly high and the hydrogen release rates at 2.5 min are low. The slightly high initial hydrogen release rate is attributed to the slightly large quantities of hydrogen desorbed from the surfaces of the particles and released from the Mg-H solid solution. MgH$_2$-15Ti has very low hydrogen release rate after 2.5 min. MgH$_2$-12Ti and MgH$_2$-6Ti have low and nearly constant hydrogen release rates from 5 min to 60 min. MgH$_2$-12Ti has the highest initial hydrogen release rate and the largest quantity of hydrogen released for 60 min, H_d (60 min). Table 2 shows the variation of H_d with t at 573 K in 1.0 bar H_2 at $n = 1$ for MgH$_2$-xTi (x = 6, 12, and 15).
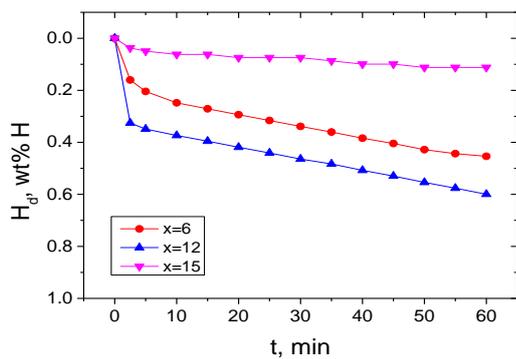
Fig. 2. Variation in the H_d vs. t curve with x at 573 K in 1.0 bar H_2 at $n = 1$ for MgH$_2$-xTi (x = 6, 12, and 15) samples

Table 2. Variation of H_d (wt.% H) with t (min) at 573 K in 1.0 bar H_2 at $n = 1 \sim 4$ for MgH$_2$-xTi (x = 6, 12, and 15)

	2.5 min	5 min	10 min	30 min	60 min
x = 6	0.16	0.20	0.25	0.34	0.45
x = 12	0.33	0.35	0.37	0.46	0.59
x = 15	0.04	0.05	0.06	0.07	0.11

Fig. 1 and Fig. 2 show that among the MgH$_2$-xTi (x = 6, 12, and 15) samples, MgH$_2$-12Ti has the highest initial hydrogen uptake and release rates and the largest H_a (60 min) and H_d (60 min). The hydrogen uptake and release properties of MgH$_2$-12Ti were studied in more detail.

Fig. 3 shows the SEM micrographs of MgH$_2$-6Ti, MgH$_2$-12Ti, and MgH$_2$-15Ti after reactive mechanical milling. The particle sizes are not homogeneous. The particles are agglomerated. MgH$_2$-12Ti has the smallest agglomerates, followed in order by MgH$_2$-6Ti and MgH$_2$-15Ti.

The variation in the H_a vs. t curve with cycle number, n, at 573 K in 12 bar H_2 for MgH$_2$-12Ti is shown in Fig. 4. At $n = 1$, the initial hydrogen uptake rate is quite high and the quantity of hydrogen absorbed for 60 min, H_a (60 min), is quite large. At $n = 1$, the hydrogen uptake rate decreases gradually as the reaction time elapses and is very low after 20 min. As n increases from one to three, the initial hydrogen uptake rate and H_a (60 min) decrease rapidly. From $n = 3$ to $n = 4$, the initial hydrogen uptake rate and H_a (60 min) increase. During vacuum pumping at 623 K after the release measurement, residual hydrogen release and

coalescence of cracks inside the particles can occur. The higher initial hydrogen uptake rate and the larger H_a (60 min) at $n = 4$ than at $n = 3$ is thought to result from shorter vacuum pumping time (1.5 h) after the release measurement of the third cycle than that (6 h) after the release measurement of the second cycle.
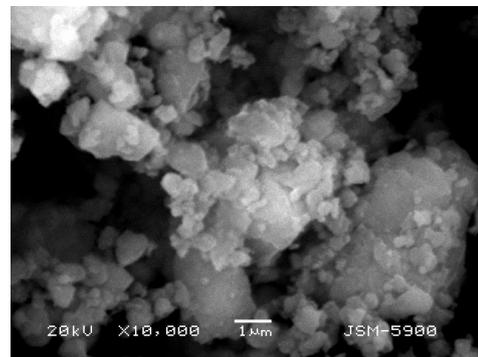
a
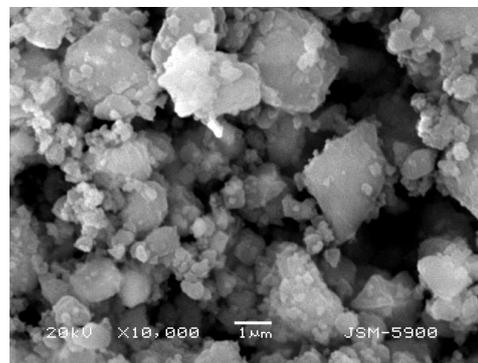
b
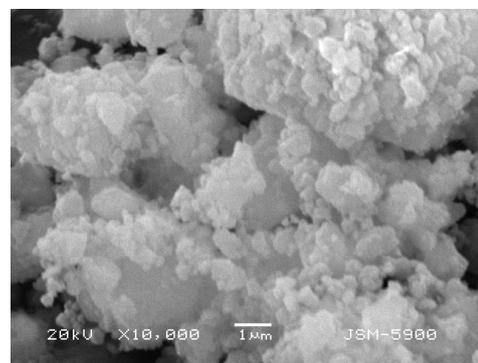
c

Fig. 3. SEM micrographs of; a – MgH$_2$-6Ti; b – MgH$_2$-12Ti; c – MgH$_2$-15Ti after reactive mechanical grinding

The general decreases in the initial hydrogen uptake rate and H_a (60 min) with the cycle number are attributed to coalescence of cracks inside the particles because the sample was maintained at the relatively high temperatures, 573 K during hydrogen uptake-release cycling and 623 K during vacuum pumping. The longer vacuum pumping time (6 h) after the release measurement of the second cycle than that (1.5 h) after the release measurement of the third cycle is thought to have caused the lower initial hydrogen uptake rate and the smaller H_a (60 min) at $n = 3$ than at $n = 4$ due to coalescence of cracks inside the particles. At $n = 1$, MgH$_2$-12Ti absorbs 4.00 wt.% H for

2.5 min and 6.39 wt.% H for 60 min. At $n = 4$, MgH$_2$-12Ti absorbs 1.66 wt.% H for 2.5 min and 3.35 wt.% H for 60 min.
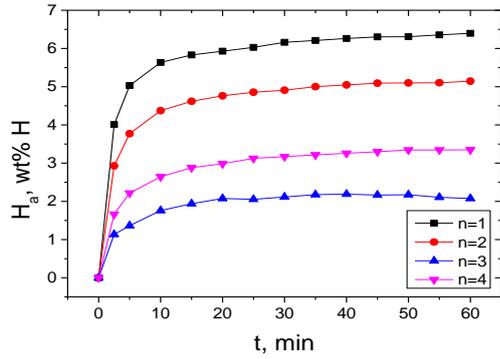
Fig. 4. Variation in the H_a vs. t curve with cycle number, n, at 573 K in 12 bar H$_2$ for MgH$_2$-12Ti

We define the quantity of hydrogen absorbed for 60 min as the effective hydrogen storage capacity. MgH$_2$-12Ti has an effective hydrogen storage capacity of 6.39 wt.% at 573 K in 12 bar H$_2$ at $n = 1$.

The variation in the H_d vs. t curve with cycle number, n, at 573 K in 1.0 bar H$_2$ for MgH$_2$-12Ti is shown in Fig. 5. At $n = 1$, the initial hydrogen release rate is slightly high and the quantity of hydrogen released for 60 min, H_d (60 min), is small. As n increases from one to three, the initial hydrogen release rate and H_d (60 min) decrease. From $n = 3$ to $n = 4$, the initial hydrogen release rate and H_d (60 min) increase. The higher initial hydrogen release rate and the larger H_d (60 min) at $n = 4$ than at $n = 3$ result from larger H_a (60 min) at $n = 4$ than at $n = 3$. The general decreases in the initial hydrogen release rate and H_d (60 min) with the cycle number are also attributed to the coalescence of cracks inside the particles because the sample was maintained at relatively high temperatures 573 K and 623 K during hydrogen uptake-release cycling. After 5 min, the hydrogen release rates are nearly constant. At $n = 1$, MgH$_2$-12Ti releases 0.33 wt.% H for 2.5 min and 0.59 wt.% H for 60 min. At $n = 4$, MgH$_2$-12Ti releases 0.28 wt.% H for 2.5 min and 0.53 wt.% H for 60 min.
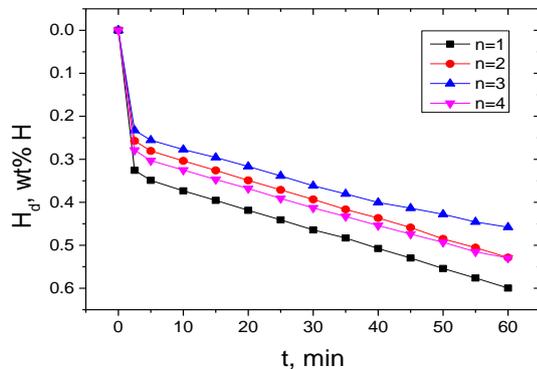
Fig. 5. Variation in the H_d vs. t curve with n at 573 K in 1.0 bar H$_2$ for MgH$_2$-12Ti

Fig. 6 shows the variation in the H_a vs. t curve with cycle number, n, at 593 K in 12 bar H$_2$ for MgH$_2$-12Ti. At $n = 1$, the initial hydrogen uptake rate is quite high and the

quantity of hydrogen absorbed for 60 min, H_a (60 min), is quite large. As n increases from one to four, the initial hydrogen uptake rate and H_a (60 min) decrease. The change in H_a (60 min) with n at 593 K is relatively small, compared with that at 573 K. The hydrogen uptake rate decreases gradually as the reaction time elapses and is very low after 20 min. At $n = 1$, MgH$_2$-12Ti absorbs 3.06 wt.% H for 2.5 min and 5.39 wt.% H for 60 min. At $n = 4$, MgH$_2$-12Ti absorbs 2.69 wt.% H for 2.5 min and 4.67 wt.% H for 60 min. Table 3 shows the variation of H_a with t at 593 K in 12 bar H$_2$ at $n = 1 \sim 4$ for MgH$_2$-12Ti. The initial hydrogen uptake rate and H_a (60 min) at $n = 1$ at 593 K are lower and smaller, respectively, than those at $n = 1$ at 573 K. The increase in temperature increases the diffusion rate of hydrogen atoms but decreases the driving force for hydrogenation (the difference between the applied hydrogen pressure and the equilibrium plateau pressure at a given temperature). We believe that the effect of the latter predominates over that of the former, leading to decreases in the initial hydrogen uptake rate and H_a (60 min) at $n = 1$ at 593 K.
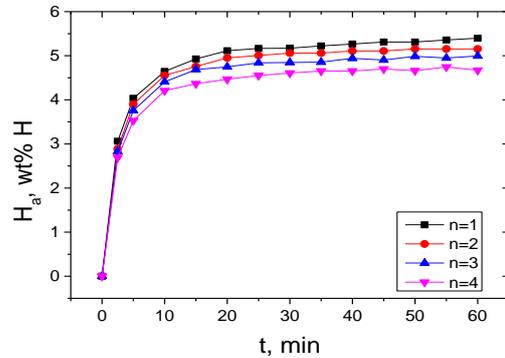
Fig. 6. Variation in the H_a vs. t curve with n at 593 K in 12 bar H$_2$ for MgH$_2$-12Ti

The variation in the H_d vs. t curve with cycle number, n, at 593 K in 1.0 bar H$_2$ for MgH$_2$-12Ti is shown in Fig. 7. At $n = 1$, the initial hydrogen release rate is slightly high and the quantity of hydrogen released for 60 min, H_d (60 min), is larger, compared with H_d (60 min) at 573 K. As n increases from one to four, the initial hydrogen release rate and H_d (60 min) decrease.

Table 3. Variation of H_a (wt.% H) with t (min) at 593 K in 12 bar H$_2$ at $n = 1 \sim 4$ for MgH$_2$-12Ti

	2.5 min	5 min	10 min	30 min	60 min
n = 1	3.06	4.03	4.64	5.17	5.39
n = 2	2.89	3.90	4.55	5.06	5.15
n = 3	2.82	3.77	4.41	4.84	4.99
n = 4	2.69	3.53	4.21	4.01	4.67

From $n = 1$ to $n = 2$, H_d (60 min) decreases sharply and from $n = 2$ to $n = 4$, H_d (60 min) decreases slowly. At 2.5 min, the hydrogen release rates are low. The hydrogen release rates increase gradually after 2.5 min and are quite high at 50 min. At $n = 1$, MgH$_2$-12Ti releases 0.44 wt.% H for 2.5 min and 1.86 wt.% H for 60 min. At $n = 4$, MgH$_2$-12Ti releases 0.37 wt.% H for 2.5 min and 1.44 wt.% H for 60 min. Table 4 shows the of H_d with t at 593 K in 1.0 bar H$_2$ at $n = 1 \sim 4$ for MgH$_2$-12Ti. The initial

hydrogen release rate and H_d (60 min) at 593 K are higher and larger, respectively, than those at 573 K. The increase in temperature increases not only the diffusion rate of hydrogen atoms but also the driving force for dehydrogenation (the difference between the equilibrium plateau pressure at a given temperature and the applied hydrogen pressure), leading to increases in the initial hydrogen release rate and H_d (60 min) at 593 K.
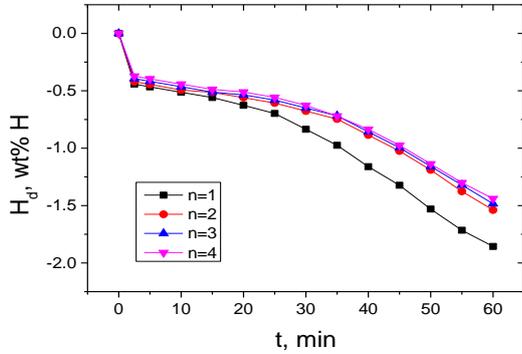
Fig. 7. Variation in the H_d vs. t curve with n at 593 K in 1.0 bar H_2 for MgH$_2$-12Ti

Table 4. Variation of H_d (wt% H) with t (min) at 593 K in 1.0 bar H_2 at $n = 1 \sim 4$ for MgH$_2$-12Ti

	2.5 min	5 min	10 min	30 min	60 min
n = 1	0.44	0.57	0.51	0.84	1.86
n = 2	0.42	0.44	0.49	0.68	1.54
n = 3	0.39	0.42	0.46	0.65	1.48
n = 4	0.37	0.39	0.44	0.63	1.44

Fig. 8 shows the SEM micrographs at various magnifications of MgH$_2$-12Ti after reactive mechanical grinding. Particle size is not homogeneous; some particles are fine and some particles are large. These particles form agglomerates. Some large particles have flat surfaces with few fine particles on the surfaces.

The SEM micrographs at various magnifications of MgH$_2$-12Ti dehydrogenated in 1.0 bar H$_2$ at $n = 4$ are shown in Fig. 9. Particle size is not homogeneous, either; some particles are fine and some particles are large. However, this sample has more homogeneous particle size than the sample after reactive mechanical grinding.
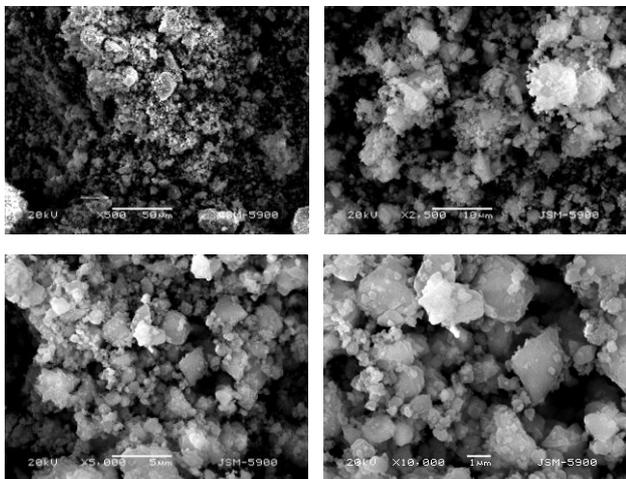
Fig. 8. SEM micrographs at various magnifications of MgH$_2$-12Ti after reactive mechanical grinding

These particles form agglomerates. Particles on the surfaces of the particles are smaller than those of the sample after reactive mechanical grinding. The agglomerates are larger than those of the sample after reactive mechanical grinding.
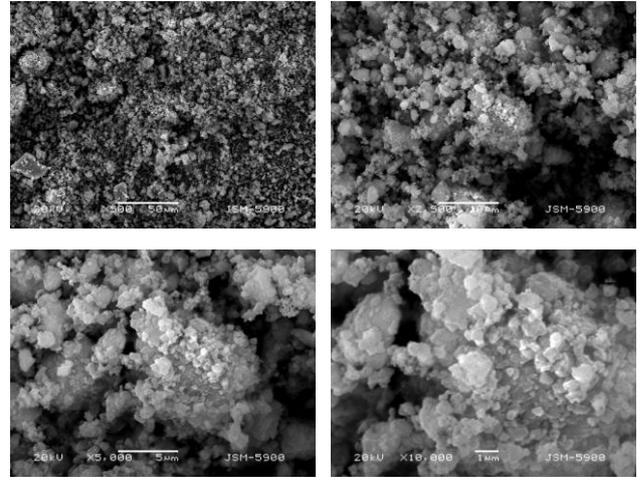
Fig. 9. SEM micrographs at various magnifications of MgH$_2$-12Ti dehydrogenated at 593 K in 1.0 bar H$_2$ at $n = 4$ after hydrogen uptake-release cycling at 593 K

Fig. 10 shows the XRD pattern of MgH$_2$-12Ti after reactive mechanical grinding. The MgH$_2$-12Ti after reactive mechanical grinding contains a large amount of β-MgH$_2$ and small amounts of Mg, γ-MgH$_2$, TiH$_{1.924}$, and MgO. This shows that most of the sample is hydrogenated to β-MgH$_2$ and that TiH$_{1.924}$ is formed by the reaction of Ti with hydrogen during milling in hydrogen. Liang et al. [7] reported that TiH$_2$ was formed after 20 h of milling of MgH$_2$ with Ti. Biasetti et al. [15, 16] reported the formation of TiH$_2$ after milling Mg with Ti in hydrogen.

The XRD pattern of MgH$_2$-12Ti dehydrogenated at 593 K in 1.0 bar H$_2$ at $n = 4$ after hydrogen uptake-release cycling at 593 K is shown in Fig. 11. The MgH$_2$-12Ti dehydrogenated at 593 K in 1.0 bar H$_2$ at $n = 4$ contains large amounts of β-MgH$_2$ and Mg and very small amounts of MgO, TiH$_{1.924}$, and Mg(OH)$_2$. The existence of large amounts of β-MgH$_2$ indicates that most of the hydrides in the sample are not decomposed.
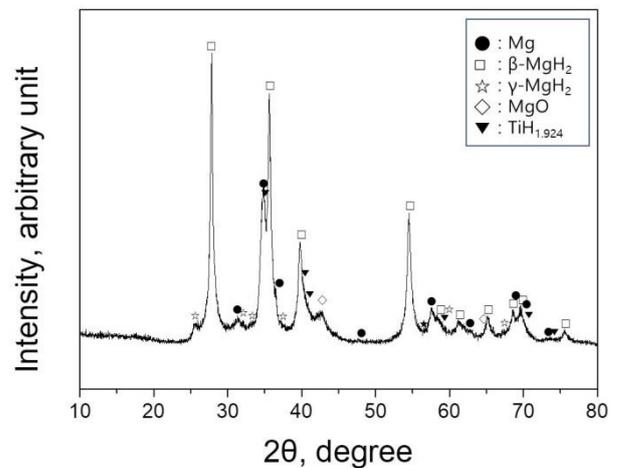
Fig. 10. XRD pattern of MgH$_2$-12Ti after reactive mechanical grinding

TiH$_{1.924}$ remains undecomposed, but γ-MgH$_2$ is not present, after the sample was dehydrogenated in 1.0 bar H$_2$ at $n = 4$. We believe that MgO was formed by the reaction with oxygen adsorbed on the particle surfaces while the sample was treated to obtain the XRD pattern. Mg(OH)$_2$ is thought to have been formed by the reaction of MgO with the water vapor adsorbed on the particle surfaces during treating the samples to obtain the XRD pattern. Liang et al. [7] reported that TiH$_2$ phase did not decompose after desorption at 573 K in 0.15 bar H$_2$. Biasetti et al. [15, 16] reported that the TiH$_2$ formed after milling remained as a stable phase after cycling. The addition of 12 wt.% Ti to MgH$_2$ decreased the theoretical hydrogen storage capacity from 7.60 wt.% to 7.15 wt.%. Some hydrogen is "trapped" in the form of TiH$_{1.924}$. The formation of TiH$_{1.924}$ decreases partly the practical reversible quantity of hydrogen (hydrogen absorbed and then released).
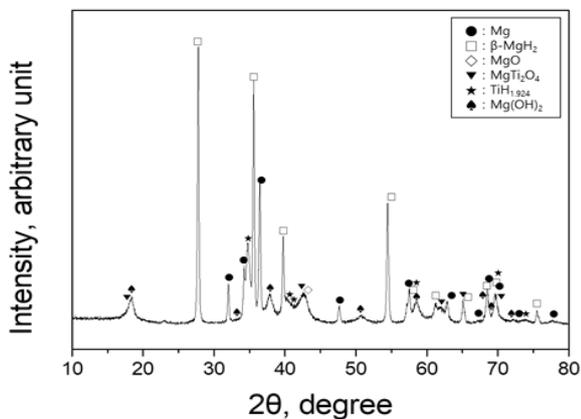
Fig. 11. XRD pattern of MgH$_2$-12Ti dehydrogenated at 593 K in 1.0 bar H$_2$ at $n = 4$ after hydrogen uptake-release cycling at 593 K

During reactive mechanical grinding of MgH$_2$ with Ti, brute forces and tensile, compressive, or shear stresses are applied to the material. These forces and stresses are believed to introduce imperfections, fabricate cracks, expose fresh and clean surfaces, decrease the particle size [21 – 26], and disperse the additive among the particles. Introduction of imperfections is considered to ease nucleation. We believe that fabricating cracks and exposing fresh and clean surfaces increase the reactivity of particles with hydrogen. Decreasing the particle size is deemed to decrease the diffusion distance of hydrogen atoms [21 – 26]. We believe that dispersing the additive and materials produced during reactive mechanical grinding among the particles prevents the particles from being coalesced during hydrogen uptake-release cycling. Decreasing the particle sizes leads to the increase in the specific surface area of the sample. The γ-MgH$_2$, TiH$_{1.924}$, and MgO formed during reactive mechanical grinding and their pulverization during reactive mechanical grinding are believed to make these effects stronger.

We believe that the hydrogen uptake-release cycling also creates defects, produces cracks and clean surfaces, and decreases particle sizes due to expansion (by hydrogen uptake) and contraction (by hydrogen release) of Mg [15 – 17]. We confirmed these effects with our result that the particles on the surfaces of relatively large particles, as

shown in Fig. 9, are smaller than those of the sample after reactive mechanical grinding, as shown in Fig. 8.

Fig. 4 – Fig. 7 show that the activation of MgH$_2$-12Ti is not necessary. The quantity of hydrogen absorbed for 2.5 min, H_a (2.5 min), H_a (60 min), the quantity of hydrogen released for 2.5 min, H_d (2.5 min), and H_d (60 min) all decrease in general as n increases, showing that the cycling performance of MgH$_2$-12Ti is poor. Even though the particles on the surfaces of the relatively large ones after four hydrogen uptake-release cycles are smaller than those of the sample after reactive mechanical grinding, as shown in Fig. 9, the general decrease in H$_a$ (2.5 min), H_a (60 min), H_d (2.5 min), and H_d (60 min) with increasing n suggests that the coalescence of cracks inside the particles occurs since the sample was maintained at relatively high temperatures (573 K and 593 K) during hydrogen uptake-release cycling. We plan to perform further studies to improve the cycling performance of MgH$_2$-12Ti in our future work.

Fig. 12 shows the H_a vs. t curves at 593 K in 12 bar H$_2$ and the H_d vs. t curves at 593 K in 1.0 bar H$_2$ at $n = 1$ for MgH$_2$ after reactive mechanical grinding (named MgH$_2$ after RMG) and MgH$_2$-12Ti. MgH$_2$ after RMG has a higher initial hydrogen uptake rate and a larger H_a (60 min) than MgH$_2$-12Ti.
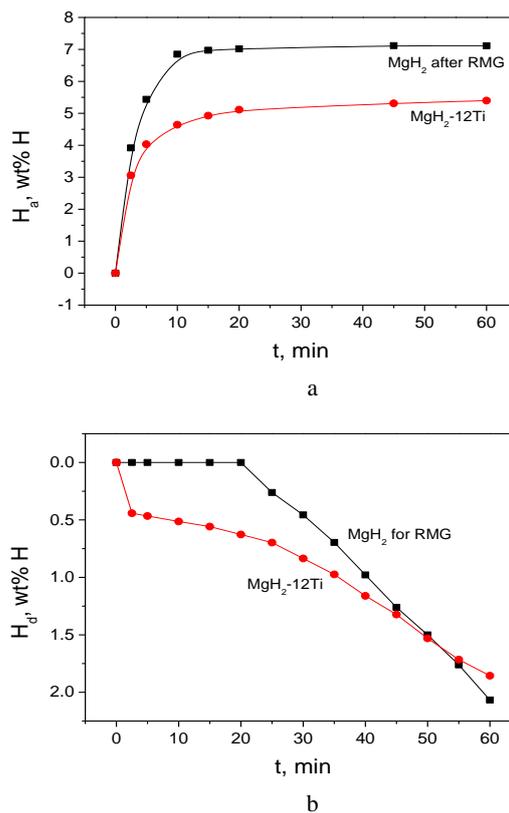
Fig. 12. a – H_a vs. t curves at 593 K in 12 bar H$_2$ and b – H_d vs. t curves at 593 K in 1.0 bar H$_2$ at $n = 1$ for MgH$_2$ after RMG and MgH$_2$-12Ti

MgH$_2$ after RMG exhibits an incubation period of about 20 min, after which MgH$_2$ after RMG releases hydrogen quite rapidly. MgH$_2$ after RMG releases 0.26 wt.% H for 25 min and 2.07 wt.% H for 60 min. The initial hydrogen release rate of MgH$_2$-12Ti is slightly high

and the hydrogen release rate of MgH_2-12Ti is low at 2.5 min. The hydrogen release rates increase gradually after 2.5 min and are quite high at 50 min. MgH_2-12Ti releases 0.44 wt.% H for 2.5 min and 1.86 wt.% H for 60 min. These results show that the addition of Ti to MgH_2 by reactive mechanical grinding facilitates the nucleation of Mg-H solid solution in the hydrogenated sample.

Rizo-Acosta et al. [10] reported that the $0.975MgH_2 + 0.025TiH_2$ nanocomposite had the highest reversible capacity of 4.9 wt.% H among $(1-y)MgH_2+yTiH_2$ nanocomposites ($y = 0$, 0.025, 0.05, 0.1, 0.2, and 0.3) which they prepared by reactive ball milling. Calizzi et al. [13] prepared Mg nanoparticles with the addition of Ti catalysts and reported that hydrogen desorption (desorption pressure = 8 mbar) and absorption (absorption pressure = 260 mbar) was achieved at 473 K in about 2000 s, while keeping a hydrogen storage capacity of 5.3 wt%. Lu et al. [14] prepared nanocrystalline Mg and 90 wt.% Mg + 10 wt.% Ti hydrogen-storage alloys by reactive mechanical grinding and hydrogen uptake-release cycling five times. 90 wt.% Mg + 10 wt.% Ti had an improved hydrogen absorptioncapacity (3.63 wt.%) compared with Mg (3.36 wt.%). MgH_2-12Ti prepared in this work has a higher hydrogen storage capacity (an effective hydrogen storage capacity of 6.39 wt.% at 573 K in 12 bar H_2 at $n = 1$) than these reported composites.

4. CONCLUSIONS

Titanium was chosen as an additive to improve the hydrogen uptake and release properties of MgH_2. 6, 12, and 15 weight percent Ti were added to MgH_2 by milling in hydrogen (reactive mechanical grinding). Among the MgH_2-xTi (x = 6, 12, and 15) samples, MgH_2-12Ti had the highest initial hydrogen uptake and release rates and the largest H_a (60 min) and H_d (60 min). The hydrogen uptake and release properties of MgH_2-12Ti were studied in more detail because it had the highest initial hydrogen uptake and release rates and the largest quantities of hydrogen absorbed and released for 60 min. At the first cycle, MgH_2-12Ti absorbed 4.01 wt.% H for 2.5 min and 6.39 wt.% H for 60 min at 573 K in 12 bar H_2, having an effective hydrogen storage capacity of 6.39 wt.%. MgH_2-12Ti released 0.44 wt.% H for 2.5 min and 1.86 wt.% H for 60 min at 593 K in 1.0 bar H_2. We believe that reactive mechanical grinding introduces imperfections, fabricates cracks, exposes fresh and clean surfaces, decreases the particle size, and disperses the additive among the particles. The γ-MgH_2, $TiH_{1.924}$, and MgO formed during reactive mechanical grinding and their pulverization during reactive mechanical grinding are believed to make these effects stronger. The hydrogen uptake-release cycling is also believed to induce effects similar to those of reactive mechanical grinding. The poor cycling performance of MgH_2-12Ti is attributed to the coalescence of cracks inside the particles because the sample was maintained at relatively high temperatures (573 K, 593 K, and 623 K) during hydrogen uptake-release cycling. We plan to perform further studies to improve the cycling performance of MgH_2-12Ti in our future work.

REFERENCES

1. **Song, M.Y., Kwak, Y.J.** Effects of $Zn(BH_4)_2$, Ni, and/or Ti Doping on the Hydrogen-Storage Features of MgH_2 *Korean Journal of Metals and Materials* 57 (3) 2019: pp. 176 – 183. https://doi.org/10.3365/KJMM.2019.57.3.176

2. **Song, M.Y., Choi, E., Kwak, Y.J.** Preparation of a Mg-Based Alloy with a High Hydrogen-Storage Capacity by Adding a Polymer CMC via Milling in a Hydrogen Atmosphere *International Journal of Hydrogen Energy* 44 (7) 2019: pp. 3779 – 3789. https://doi.org/10.1016/j.ijhydene.2018.12.081

3. **Song, M.Y., Choi, E., Kwak, Y.J.** Increase in the Dehydrogenation Rate of Mg-CMC (Carboxymethylcellulose, Sodium Salt) by Adding Ni via Hydride-Forming Milling *Metals and Materials International* 25 2019: pp. 516 – 527. https://doi.org/10.1007/s12540-018-0188-2

4. **Song, M.Y., Kwak, Y.J., Lee, S.H.** $TiCl_3$ and Ni-Added Mg Prepared by Reactive Mechanical Grinding Processing and Comparison with Fe_2O_3 and Ni-Added Mg *Journal of Ceramic Processing Research* 20 (2) 2019: pp. 173 – 181. https://doi.org/10.36410/jcpr.2019.20.2.173

5. **Song, M.Y., Choi, E., Kwak, Y.J.** Nickel, Graphene, and Yttria-Stabilized Zirconia (YSZ)-Added Mg by Grinding in Hydrogen Atmosphere for Hydrogen Storage *Metals* 9 (12) 2019: pp. 1 – 16. https://doi.org/10.3390/met9121347

6. **Song, M.Y., Choi, E., Kwak, Y.J.** Hydrogenation and Dehydrogenation Behaviors of Mg_2Ni Synthesized by Sintering Pelletized Mixtures under an Ar Atmosphere *Journal of Nanoscience and Nanotechnology* 19 (10) 2019: pp.6571 – 6579. https://doi.org/10.1166/jnn.2019.17082

7. **Liang, G., Huot, J., Boily, S., Van Neste, A., Schulz, R.** Catalytic Effect of Transition Metals on Hydrogen Sorption in Nanocrystalline Ball Milled MgH_2–Tm (Tm=Ti, V, Mn, Fe and Ni) Systems *Journal of Alloys and Compounds* 292 (1 – 2) 1999: pp. 247 – 252. https://doi.org/10.1016/S0925-8388(99)00442-9

8. **Asano, K., Etsuo Akiba, E.** Direct Synthesis of Mg–Ti–H FCC Hydrides from MgH_2 and Ti by Means of Ball Milling *Journal of Alloys and Compounds* 481 (1 – 2) 2009: pp. L8 – L11. https://doi.org/10.1016/j.jallcom.2009.02.152

9. **Korablov, D., Torben, F.B., Jensen, R.** Kinetics and Thermodynamics of Hydrogenation-Dehydrogenation for Mg-25%TM (TM = Ti, Nb or V) Composites Synthesized by Reactive Ball Milling in Hydrogen *International Journal of Hydrogen Energy* 43 (34) 2018: pp. 16804 – 16814. https://doi.org/10.1016/j.ijhydene.2018.05.091

10. **Rizo-Acosta, P., Cuevas, F., Latroche, M.** Optimization of TiH_2 Content for Fast and Efficient Hydrogen Cycling of MgH_2-TiH_2 Nanocomposites *International Journal of Hydrogen Energy* 43 2018: pp. 16774 – 16781. https://doi.org/10.1016/j.ijhydene.2018.04.169

11. **Maweja, K., Phasha, M., van der Berg, N.** Microstructure and Crystal Structure of an Equimolar Mg–Ti Alloy Processed by Simoloyer High-Energy Ball Mill *Powder Technology* 199 (3) 2010: pp. 256 – 263.
https://doi.org/10.1016/j.powtec.2010.01.014

12. **Korablov, D., Besenbacher, F., Jensen, T.R.** Ternary Compounds in the Magnesium–Titanium Hydrogen Storage System *International Journal of Hydrogen Energy* 39 (18) 2014: pp. 9700 – 9708.
https://doi.org/10.1016/j.ijhydene.2014.03.141

13. **Calizzi, M., Chericoni, D., Jepsen, L.H., Jensen, T.R., Pasquini, L.** Mg–Ti Nanoparticles with Superior Kinetics for Hydrogen Storage *International Journal of Hydrogen Energy* 41 2016: pp. 14447 – 14454.
https://doi.org/10.1016/j.ijhydene.2016.03.071

14. **Lu, W.C., Ou, S.F., Lin, M.H. Wong, M.F.** Hydriding Characteristics of Mg–Ti Alloys Prepared by Reactive Mechanical Grinding and Hydrogen Pulverization *Journal of Alloys and Compounds* 664 2016: pp. 193 – 198.
https://doi.org/10.1016/j.jallcom.2015.12.064

15. **Biasetti, A., Meyer, M., Mendoza Zelis, L.** Formation Kinetics and Microstructure of Mg–Ti Hydrides Made by Reactive Ball Milling *International Journal of Hydrogen Energy* 39 2014: pp. 8767 – 8771.
https://doi.org/10.1016/j.ijhydene.2013.12.034

16. **Biasetti, A., Meyer, M., Mendoza Zelis, L.** Hydriding Kinetics of $MgTiH_2$ Fine Dispersions Obtained by Mechanosynthesis *Powder Technology* 307 2017: pp. 145 – 152.
https://doi.org/10.1016/j.powtec.2016.11.026

17. **Daryani, M., Simchi, A., Sadati, M., Mdaah Hosseini, H., Targholizadeh, H., Khakbiz, M.** Effects of Ti-Based Catalysts on Hydrogen Desorption Kinetics of Nanostructured Magnesium Hydride *International Journal of Hydrogen Energy* 39 2014: pp. 21007 – 21014.
https://doi.org/10.1016/j.ijhydene.2014.10.078

18. **Alsabawi, K., Gray, E., Mac, A., Webb, C.J.** The Effect of Ball-Milling Gas Environment on the Sorption Kinetics of MgH_2 with/without Additives for Hydrogen Storage *International Journal of Hydrogen Energy* 44 (5) 2019: pp. 2976 – 2980.
https://doi.org/10.1016/j.ijhydene.2018.12.026

19. **Park, H.R., Kwak, Y.J., Song, M.Y.** Increase in the Hydrogen-Sorption Rates and the Hydrogen-Storage Capacity of MgH_2 by Adding a Small Proportion of $Zn(BH_4)_2$ *Korean Journal of Metals and Materials* 55 (9) 2017: pp. 657 – 663.
https://doi.org/10.3365/KJMM.2017.55.9.657

20. **Hong, S.H., Kwak, Y.J., Song, M.Y.** Enhancement of the Hydrogen-Storage Characteristics of Mg by Adding Mg_2Ni and Ni to MgH_2 via High Energy Ball Milling in Hydrogen Atmosphere *Korean Journal of Metals and Materials* 56 (1) 2018: pp. 59 – 65.
https://doi.org/10.3365/KJMM.2018.56.1.59

21. **Hong, S.H., Song, M.Y.** Hydrogen Absorption and Release Properties of MgH_2, Mg_2Ni, and Ni-added Mg via Reactive Mechanical Grinding *Korean Journal of Metals and Materials* 56 (2) 2018: pp. 155 – 162.
https://doi.org/10.3365/KJMM.2018.56.2.155

22. **Song, M.Y., Kwak, Y.J.** Comparison of the Hydrogen Release Properties of $Zn(BH_4)_2$-Added MgH_2 Alloy and $Zn(BH_4)_2$ and Ni-added MgH_2 Alloy *Korean Journal of Metals and Materials* 56 (3) 2018: pp. 244 – 251.
https://doi.org/10.3365/KJMM.2018.56.3.244

23. **Song, M.Y., Choi, E., Kwak, Y.J.** Development of a Mg-Based Alloy with a Hydrogen-Storage Capacity of 7 wt.% by Adding a Polymer CMC via Transformation-Involving Milling *Korean Journal of Metals and Materials* 56 (5) 2018: pp. 392 – 399.
https://doi.org/10.3365/KJMM.2018.56.5.392

24. **Song, M.Y., Kwak, Y.J., Choi, E.** Hydrogen Storage Properties of Mg-Graphene Composites *Korean Journal of Metals and Materials* 56 (7) 2018: pp. 524 – 531.
https://doi.org/10.3365/KJMM.2018.56.7.524

25. **Song, M.Y., Kwak, Y.J.** Hydrogen Uptake and Release Characteristics of $Mg-xTaF_5-xVCl_3$ (x = 1.25, 2.5, and 5) *Korean Journal of Metals and Materials* 56 (8) 2018: pp. 611 – 619.
https://doi.org/10.3365/KJMM.2018.56.8.611

26. **Song, M.Y., Choi, E., Kwak, Y.J.** Raising the Dehydrogenation Rate of a Mg-CMC (Carboxymethylcellulose, Sodium Salt) Composite by Alloying Ni via Hydride-Forming Milling *Korean Journal of Metals and Materials* 56 (8) 2018: pp. 620 – 627.
https://doi.org/10.3365/KJMM.2018.56.8.620